Accurate Estimation of the Error Probability in the Presence of In-Band Crosstalk Noise in WDM Networks

Thomas Kamalakis, Thomas Sphicopoulos, *Member, IEEE,* and Manolis Sagriotis

***Abstract*—In-band crosstalk noise can pose important limitations in wavelength-division-multiplexing (WDM) optical networks. This paper describes a model that takes into account the statistical behavior of in-band crosstalk noise accurately and that can be used to estimate the error probability (EP) in a WDM receiver. It is based on the formulation of the moment-generating function of the decision variable in terms of a double integral, which allows the inclusion of the crosstalk–crosstalk noise, which was previously neglected in the literature. The optical amplifier noise and the electrical receiver noise are also incorporated, and the model is used to assess the implications of the crosstalk–crosstalk contribution. With the aid of some examples, it is shown that the crosstalk–crosstalk noise can influence the value of the EP, change the optimum receiver threshold, and introduce some power penalty.**

***Index Terms*—Crosstalk, error analysis, optical receivers, wavelength-division multiplexing (WDM).**

I. Introduction

WAVELENGTH-DIVISION multiplexing (WDM) [1] is a promising technology for the realization of optical networks because it allows the full utilization of the large bandwidth of the optical fiber. In WDM networks, wavelength multiplexers and demultiplexers play a central role by allowing the combination and separation, respectively, of the wavelength channels. However, as a result of their imperfect filtering characteristics, the separation of the wavelengths at the receiver may not be ideal, leading to performance degradation due to crosstalk noise. Crosstalk noise is divided into two categories: in-band and out-band crosstalk noise. Out-band crosstalk noise occurs when the carrier frequencies of the signal and the interferer differ by an amount greater than the bandwidth of the electronic filter, while in-band crosstalk noise occurs otherwise. Out-band crosstalk noise can be removed by additional filtering at the receiver. In-band crosstalk, however, cannot be removed and can therefore degrade the error probability (EP) of the system [2].

Several approaches have been proposed in the literature in order to assess the implications of in-band crosstalk on system performance. In order to evaluate the EP, the statistical behavior of the decision variable at the receiver must be considered. If the receiving photodiode is assumed to act as a square law device, then the decision variable can be written as the sum of three contributions: the signal–signal beating, the signal–crosstalk beating noise, and the crosstalk–crosstalk beating noise. When only the signal–signal contribution and the signal–crosstalk noise is assumed, then in the case of a large number of interfering channels, the probability density function (pdf) of the decision variable can be assumed Gaussian and the EP can be easily computed. Despite its simplicity, the Gaussian model cannot accurately describe the signal–crosstalk noise, especially when the number of interfering components is not large [3]. Since the exact pdf of the crosstalk noise is not known in closed form, an alternative is to use the saddle point method for the evaluation of the EP [4]. The saddle point method computes the EP from the moment-generating function (MGF) of the decision variable at the receiver. Most of the previous models neglected the crosstalk–crosstalk contribution at the receiver, in which case the MGF of the decision variable is known in closed form and the EP can be easily computed numerically [3], [5]. Other analyses assumed that the components of the crosstalk–crosstalk contribution are mutually independent and uncorrelated from the signal–crosstalk contribution [6], which may not provide an accurate description of the situation since both of these contributions originate from the same optical crosstalk noise.

In [7], it is noted that the inclusion of the crosstalk–crosstalk beating term can affect the pdf of the crosstalk noise. However, the influence of the crosstalk–crosstalk noise in the value of the EP was not considered in the previously mentioned study. Moreover, the calculation of the MGF through which the pdf was computed was accomplished using M-dimensional numerical integration, where M is the number of interfering channels. As a result, the calculation of the MGF can prove a time-consuming task if the number of interferers M is large. The implications of the crosstalk–crosstalk noise in the performance of the system were considered in [8], assuming that the number of interferers is infinite ($M \to \infty$). In the absence of optical amplification, the decision variable was shown to follow a noncentral chi-square distribution, whose MGF is known in closed form. Using the saddle-point approximation, it was shown that even in the presence of optical amplification, the crosstalk–crosstalk noise can significantly affect the value of the EP, can change the value of the optimum receiver threshold, and can also introduce some power penalty.

In this paper, an efficient method for the calculation of the MGF of the decision variable D is presented in the practical case where the number of interferers M is finite. Using certain symmetrical properties of D, it is shown that in the absence of optical amplification and electrical noise, the MGF $M(s)$

Manuscript received February 24, 2003; revised June 9, 2003.

The authors are with the Department of Informatics and Telecommunications, University of Athens, Athens GR-15784, Greece.

Digital Object Identifier 10.1109/JLT.2003.816848

of D can be expressed in terms of a double integral. For negative arguments ($s < 0$) it is shown that this double integral reduces to a simple Sommerfeld integral that can be computed efficiently using the saddle-point approximation. For positive arguments ($s > 0$), an efficient numerical integration procedure is described for the evaluation of the MGF. The model is then extended to take into account both the amplified spontaneous emission (ASE) noise of the optical amplifiers and the electrical noise of the receiver. Using this model, the influence of the crosstalk–crosstalk noise is discussed. It is shown that, as in the case of $M \to \infty$, the crosstalk–crosstalk noise can strongly influence the performance of the system and should be taken into account in system design.

The rest of the paper is organized as follows. In Section II, the evaluation of the EP from the MGF of the decision variable using the saddle-point method is briefly reviewed. In Section III, the crosstalk noise is related to the decision variable at the receiver. Using the results of Section III, a double integral formulation for the MGF is derived in Section IV, and it is shown that for negative arguments, this formulation can be further reduced to a single Sommerfeld-type integral, which can be computed efficiently using the saddle-point approximation. An efficient method for the calculation of the MGF for positive arguments is also presented. In Section V, the accuracy of the calculated MGF is discussed, and in Section VI, the model is extended to include both the ASE noise of the optical amplifiers and the electrical noise of the receiver. Using the extended model, the importance of the crosstalk–crosstalk noise in a WDM receiver is analyzed in Section VII.

II. Computation of the EP From the MGF

If the MGF of the decision variable is known in closed form or can be accurately computed numerically, then the saddle point method can be used to evaluate the value of the EP [4, Ch. 5]. More specifically, let D be the decision variable at the receiver and $M_{D|1}(s)$ the conditional MGF of D, given that the signal bit is $b_s = 1$. If

$$W_1(s) = \ln M_{D|1}(s) - as + \ln|s| \tag{1}$$

where a is the decision threshold at the receiver, then by locating the saddle point s_1 of $W_1(W_1'(s_1) = 0)$ which is found on the negative real axis [4, Chp. 5], the error probability P_{e1} in the case $b_s = 1$ is approximately given by

$$P_{e1} = P(D \le a \mid b_s = 1) \cong \frac{\exp(W_1(s_1))}{\sqrt{2\pi W_1''(s_1)}}. \tag{2}$$

A similar procedure can be carried out when the signal bit is $b_s = 0$. If $M_{D|0}(s)$ is the conditional MGF of D given that $b_s = 0$ and

$$W_0(s) = \ln M_{D|0}(s) - as + \ln|s| \tag{3}$$

then, by locating the saddle point s_0 of $W_0(s)$ on the positive real axis, the error probability P_{e0} given that $b_s = 0$ is approximately given by

$$P_{e0} = P(D \ge a \mid b_s = 0) \cong \frac{\exp(W_0(s_0))}{\sqrt{2\pi W_0''(s_0)}}. \tag{4}$$

After calculating P_{e0} and P_{e1}, the EP at the receiver can be calculated as $\mathrm{EP} = 1/2(P_{e0} + P_{e1})$.

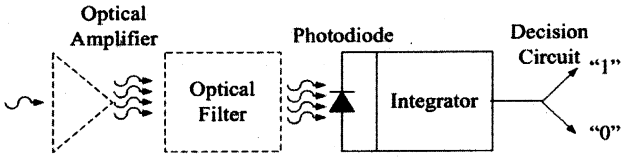

Fig. 1. Typical receiver diagram.

III. Relation Between the Decision Variable and the Crosstalk Noise

In this section, an expression relating the decision variable D (without the influence of the ASE and thermal noises) with the amplitudes and the phases of the signal and the interferers will be given. This expression will subsequently be used to formulate the MGF of the decision variable in terms of a double integral. In an optical receiver, without optical preamplification, the complex envelope $E(t)$ of the optical field at the input of the receiving photodiode is given by the sum of the signal ($m = 0$) and the noise components ($m \ge 1$)

$$E(t) = g_0(t)\exp(j\phi_0) + \sum_{m\ge 1} g_m(t)\exp(j\phi_m). \tag{5}$$

In (5), the functions $g_m(t)$ are the pulse shapes of the signal ($m = 0$) and the crosstalk components ($m \ge 1$). The random phases ϕ_m describe the phase noise of the signal and the crosstalk components. If the noise components and the signal all originate from different laser sources, as in the case of an arrayed-waveguide grating (AWG) interconnection [3], then the phases ϕ_m are all independent of each other. The phase noises are Gaussian but can be modeled as uniformly distributed inside $[-\pi, \pi]$ at the incoherent crosstalk regime. It should also be mentioned that the signal and the crosstalk noise components in (5) are assumed to be copolarized and that the bits of the interfering channels are all "1." This clearly represents a worst case scenario.

A typical receiver diagram of a direct detection amplitude-shift-keying (ASK) system is given in Fig. 1. The photocurrent $i(t)$, which is induced in the photodiode by the optical field, is given by

$$i(t) = \frac{\eta}{2hf_0}|E(t)|^2 \ \text{(photoelectrons/s)}. \tag{6}$$

In (6), η is the quantum efficiency of the photodetector, h is Planck's constant, and f_0 is the central frequency of the optical field. The effect of the electrical noise is neglected in (6). To avoid carrying out the factor $\eta/(2hf_0)$ in further calculations, the optical field is normalized so that $\eta/(2hf_0) = 1$. By replacing (5) with (6), the following expression is obtained for the photocurrent

$$i(t) = \sum_{m\ge 0}\sum_{n\ge 0} g_m(t)g_n(t)\exp(j(\phi_m - \phi_n)). \tag{7}$$

It can be assumed that the signal pulses have all the same shape, i.e., $g_m(t) = c_m g(t)$, where c_m is the amplitude of optical crosstalk noise component m. In the case the signal bit is $b_s = 0$ and if a perfect extinction ratio is assumed, then $c_0 = 0$. Note that if the energy of the pulse $g(t)$ is equal to unity ($\int_0^T |g(t)|^2 = 1$), then c_0^2 is equal to the signal energy inside the bit duration

T. In the same way if $m > 0$ then c_m^2 is equal to the energy of the interfering channel m. The decision variable is given by

$$D(T) = \int_0^T i(t)h(T-t)dt \tag{8}$$

where $h(t)$ is the impulse response of the receiver filter and T is the bit duration. If the electronic filter is assumed to be a finite-time integrator (integrate and dump filter) then $h(t) = 1$ for t inside [0, T]. The amplitude of $h(t)$ is chosen equal to 1 inside [0, T] in accordance with [4, pp. 106–107]. If one wishes the electronic filter to have unity gain at dc, $h(t)$ must equal $1/T$ inside [0, T]. This simply results in a different normalization of the signal and noise power and does not affect the final results. Using (7) and carrying out the integration in (8)

$$\begin{aligned} D = D(T) &= \sum_{n\geq 0}\sum_{m\geq 0} c_m c_n \exp\left(j\left(\phi_m - \phi_n\right)\right) \\ &= c_0^2 + 2\sum_{m\geq 1} c_m c_0 \cos\left(\phi_m - \phi_0\right) \\ &\quad + \sum_{n\geq 1}\sum_{m\geq 1} c_m c_n \exp\left(j\left(\phi_m - \phi_n\right)\right). \end{aligned} \tag{9}$$

Equation (9) is the desired expression relating the decision variable D of an optical receiver with the amplitudes and phases of the signal and the crosstalk noise components. Inspecting the last equality of (9), it can be deduced that the decision variable D can be decomposed into three parts: the signal–signal beating term (c_0^2), the signal–crosstalk beating term (single sum), and the crosstalk–crosstalk beating term (double sum). Note that if the crosstalk–crosstalk beating term is ignored, then the MGF of D can be written in closed form [3]

$$M(s) = E\left\{e^{sD}\right\} \cong M_n(s) = \exp\left(c_0^2 s\right)\prod_{m\geq 1} I_0\left(2c_m c_0 s\right). \tag{10}$$

Here, $E\{\cdot\}$ denotes expected value, and $M_n(s)$ is the MGF of D without the crosstalk–crosstalk contribution and the influence of the ASE and electrical noises. The function I_0 is the modified Bessel function of zero order [9, Ch. 11]. If the crosstalk–crosstalk noise is not neglected however, there is no closed form formula for $M(s)$. In this case, for finite M, the MGF can be computed numerically, from the M-dimensional integral [7]

$$\begin{aligned} M(s) = \frac{1}{(2\pi)^M}\int_{-\pi}^{\pi} d\psi_1 \cdots \int_{-\pi}^{\pi} d\psi_M \\ \cdot \exp\left(s\sum_{m,n=0}^{M} c_m c_n e^{j(\psi_m - \psi_n)}\right). \end{aligned} \tag{11}$$

As shown in [7], although D depends on $M+1$ random variables ($\phi_0, \ldots, \phi_M$), one can reduce the dimension of integration by 1. This can be done by integrating with respect to the variables $\psi_m = \phi_m - \phi_0$ where $m > 0$. As M begins to increase however, the M-dimensional numerical integration can become quite a time-consuming task, which may not provide very accurate results. In the next section, an alternative double integral formulation for $M(s)$ will be presented, which can be used to calculate $M(s)$ more efficiently and accurately.

IV. Formulation of the MGF of D Using a Double Integral

In this section, two auxiliary random variables R and V will be defined, and the MGF $M(s)$ of D when the crosstalk–crosstalk noise is included will be expressed in terms of these variables instead of the ϕ_m. This will result in a two-dimensional (2-D) integral formulation for $M(s)$ instead of an M-dimensional one. Let R and V be defined as

$$R = \sum_{m\geq 0} c_m \cos\phi_m, \quad V = \sum_{m\geq 0} c_m \sin\phi_m. \tag{12}$$

Using (9), it is easy to prove that

$$D = R^2 + V^2. \tag{13}$$

As will be shown next, the joint MGF $M_{RV}(js_r, js_v)$ of R and V can be expressed in closed form and depends only on $x = (s_r^2 + s_v^2)^{1/2}$. As a result of this, the joint pdf $f_{RV}(r, v)$ will be expressed as a Hankel transform of M_{RV}. Using this expression of f_{RV}, the MGF of D will then be expressed in terms of a 2-D integral of a function also known in closed form.

A. Joint MGF of R and V

The joint MGF $M_{RV}(js_r, js_v)$ of R and V is given by

$$\begin{aligned} M_{RV}\left(js_r, js_v\right) &= E\left\{\exp\left(js_r R + js_v V\right)\right\} \\ &= E\left\{\exp\left(\sum_m jc_m\left(s_r\cos\phi_m + s_v\sin\phi_m\right)\right)\right\}. \end{aligned} \tag{14}$$

Substituting $x = (s_r^2 + s_v^2)^{1/2}$ and $\theta = \tan^{-1}(s_r/s_v)$ in (14) obtains the result

$$M_{RV}\left(js_r, js_v\right) = E\left\{\exp\left(jx\sum_m c_m\cos\left(\phi_m - \theta\right)\right)\right\}. \tag{15}$$

Since the phases ϕ_m are uniformly distributed in $[-\pi, \pi]$, the MGF of $\cos(\phi_m - \theta)$ is given by $E\{\exp(jb\cos(\phi_m - \theta))\} = E\{\exp(jb\cos\phi_m)\} = J_0(b)$, where J_0 is the Bessel function of zero order [9, Ch. 11]. Therefore, since the ϕ_m are independent

$$M_{RV}\left(js_r, js_v\right) = M_c(x) = \prod_{m\geq 0} J_0\left(c_m x\right). \tag{16}$$

In (16) and throughout the paper, all the interfering bits are assumed to be 1, which represents a worst case scenario. If, instead, the interfering bits are assumed to take the values 1 and 0 with equal probability, then it is easy to show that the theory presented subsequently still applies if the function $M_c(x)$ is written as a product of the functions $1/2(1+J_0(c_m x))$ instead of $J_0(c_m x)$. From (16), it is deduced that the joint MGF M_{RV} of R and V depends only on $x = (s_r^2 + s_v^2)^{1/2}$.

B. Joint pdf of R and V

The joint pdf $f_{RV}(r, v)$ of R and V is given by the inverse Fourier transform of $M_{RV}(js_r, js_v)$

$$\begin{aligned} f_{RV}(r,v) = \frac{1}{4\pi^2}\int_{-\infty}^{+\infty}\int_{-\infty}^{+\infty} M_{RV}\left(js_r, js_v\right) \\ \cdot e^{-j(s_r r + s_v v)} ds_r ds_v. \end{aligned} \tag{17}$$

Changing the variables of integration to x and θ

$$f_{RV}(r,v)=\frac{1}{4\pi^2}\int_0^{+\infty} xM_c(x)\int_0^{2\pi} e^{-jx\rho\cos(\theta-\psi)}d\theta dS \quad (18)$$

where $\rho=(r^2+v^2)^{1/2}$ and $\psi=\tan^{-1}(r/v)$. Using the integral representation of the Bessel function J_0 [9, Sec. 9.1.21]

$$\int_0^{2\pi} d\theta e^{-jx\rho\cos(\theta-\psi)}=2\pi J_0(x\rho) \quad (19)$$

the double integral of (18) is written as

$$f_{RV}(r,v)=f_{RV}(\rho)=\frac{1}{2\pi}\int_0^{+\infty} M_c(x)J_0(x\rho)xdx. \quad (20)$$

Equation (20) states the fact that $f_{RV}(\rho)$ and $M_c(x)$ are related through a Hankel transform pair.

C. MGF of $D=R^2+V^2$

The MGF of D (without the electrical noise contribution) is given by

$$M(s)=E\left\{e^{s(R^2+V^2)}\right\}=\int_{-\infty}^{+\infty}\int_{-\infty}^{+\infty} e^{s(r^2+v^2)} \cdot f_{RV}(r,v)drdv. \quad (21)$$

Changing the integration variables from (r,v) to (ρ,ψ) defined in Section IV-B, (21) is reduced to

$$M(s)=2\pi\int_0^{+\infty}\rho e^{s\rho^2}f_{RV}(\rho)d\rho. \quad (22)$$

Substituting (20) in (22), the following expression for $M(s)$ is obtained:

$$M(s)=\int_0^{+\infty}\rho e^{s\rho^2}\int_0^{+\infty} xM_c(x)J_0(x\rho)d\rho dx. \quad (23)$$

Note that $f_{RV}(r,v)=f_{RV}(x)$ is directly related to the pdf $f_D(d)$ of $D=R^2+V^2$. Indeed, using the transformation $D=R^2+V^2, W=\tan^{-1}(R/V)$, where $W\in[0,2\pi]$ and applying the theorem of transformation of random variables, one can easily show that

$$f_D(d)=\frac{f_{RV}(\sqrt{d})}{2}. \quad (24)$$

Since the decision variable D is given by (9), it is easy to see that $0\le D\le L^2$, where

$$L=\sum_{m=0}^{M}c_m=c_0+\sum_{m=1}^{M}c_m. \quad (25)$$

Therefore, since the value of D can not exceed L^2, $f_D(d)=0$ for $d>L^2$ and using (24), it is deduced that $f_{RV}(x)=0$ for $x>L$. As a consequence, the upper limit of integration in (22) can be set to L instead of $+\infty$, and (23) can be written as

$$M(s)=\int_0^{+\infty} dxM_c(x)x\int_0^{L} d\rho J_0(x\rho)\rho e^{s\rho^2}\ (s>0). \quad (26)$$

The 2-D integral formulation of $M(s)$ in (26) will prove useful for the computation of the MGF when $s>0$.

The fact that $f_{RV}(x)=0$ for $x>L$ can also be derived by directly substituting $M_c(x)$ from (16) into (20), in which case $f_{RV}(\rho)$ is given by

$$f_{RV}(\rho)=\frac{1}{2\pi}\int_0^{+\infty} J_0(c_0x)\cdots J_0(c_Mx)\,J_0(x\rho)xdx.$$

This integral is known to be zero [10, Sec. 6.573], for $\rho\ge L=c_0+\cdots+c_M$. When $s<0$, the order of integration in (23) can be changed, and (23) can be written in a similar form

$$M(s)=\int_0^{+\infty} dxM_c(x)x\int_0^{+\infty} d\rho J_0(x\rho)\rho e^{s\rho^2}\ (s>0). \quad (27)$$

D. Evaluation of $M(s)$ for Negative Argument ($s<0$)

The double integral in (27) can be reduced to a single one, since the inner integral is known in closed form [10, 6.631.4] for $s<0$

$$\int_0^{+\infty} d\rho J_0(x\rho)\rho e^{s\rho^2}=-\frac{1}{2s}e^{x^2/(4s)}. \quad (28)$$

By substituting (16) and (28) into (27), $M(s)$ is written as

$$M(s)=-\frac{1}{2s}\int_0^{+\infty} xJ_0(c_Mx)\cdots J_0(c_0x)\,e^{x^2/(4s)}dx. \quad (29)$$

Equation (29) holds for $s<0$ which is the interval in which $M(s)$ must be known in order to evaluate P_{e1} using (2). The path of integration of (29) can be extended in the entire real x axis, if the Bessel function $J_0(c_0x)$ is replaced by the Hankel function $H_0^{(1)}(c_0x)$ and the integral is divided by two. This is a standard practice in electromagnetism, where integrals of similar type often occur in the computation of Green's function in a layered medium [11]. In doing so, (29) is reduced to

$$M(s)=-\frac{1}{4s}\int_{-\infty}^{+\infty} xJ_0(c_Mx)\cdots H_0^{(1)}(c_0x)\,e^{x^2/(4s)}dx. \quad (30)$$

Integrals of the type of (30) are known as Sommerfeld integrals. The amplitude of the signal c_0 is in general much larger than the amplitudes of the interferers $c_m(m>1)$, and therefore, the saddle-point approximation can be used in order to evaluate

(30) with high accuracy. Since $c_0 \gg c_m$, one can use the asymptotic form of the Hankel function [9, Sec. 9.2.3], as follows:

$$H_0^{(1)}(c_0 x) \cong \sqrt{\frac{2}{\pi c_0 x}} e^{j(c_0 x - \pi/4)}. \tag{31}$$

Let the function $F(y)$ be defined by

$$F(y) = \prod_{m=1}^{M} I_0(c_m y) \exp\left(-\frac{y^2}{4s} - c_0 y\right). \tag{32}$$

Using (31) and (32), one can approximate (30) as

$$M(s) \cong \frac{-j\sqrt{2}}{4s\sqrt{\pi c_0}} \int_{-j\infty}^{+j\infty} dy \sqrt{y} e^{f(y)} \tag{33}$$

where $f(y) = \ln(F(y))$. The saddle point y_s of $f(y)$ can be located by solving numerically the equation $f'(y) = 0$. The derivative of $f(y)$ can be computed either analytically or numerically. The value of the integral in (33) is approximately given by the contribution of the neighboring points of y_s on the steepest descent path passing through y_s, which is given by [12, Ch. 6]

$$\int_{-j\infty}^{+j\infty} \sqrt{y} e^{f(y)} dy \cong \sqrt{\frac{-2\pi y_s}{f''(y_s)}} e^{f(y_s)}. \tag{34}$$

Using (30)–(34), $M(s)$ can be approximately written as

$$M(s) \cong \frac{1}{2|s|} \sqrt{\frac{x_s}{c_0 f''(y_s)}} e^{f(y_s)}. \tag{35}$$

Since $f(y)$ is known in closed form and $f''(y)$ can be computed either analytically or numerically, (33) can be used to estimate the MGF of D once the saddle point y_s is located. The error probability P_{e1} in the case where the signal bit is $b_s = 1$ can then be computed from $M(s)$ using the method outlined in Section II.

E. Evaluation of $M(s)$ for Positive Argument ($s > 0$)

In the case where $s > 0$, the 2-D integral formulation of $M(s)$ cannot be reduced further, since the inner integral of (26) is not known in closed form. To facilitate the numerical integration of (26), we define the function $G(z, s, L)$ as

$$G(z, s, L) = \int_0^L d\rho H_0^{(1)}(z\rho) \rho e^{s\rho^2}. \tag{36}$$

As shown in Appendix A, an asymptotic closed form for $G(z, s, L)$ valid for large complex z is

$$G(z, s, L) \cong \frac{L}{z} H_1^{(1)}(zL) e^{sL^2} + j\frac{2}{z^2}. \tag{37}$$

Since $\mathrm{Re}\{H_0^{(0)}(t)\} = J_0(t)$ for $t \in \Re$, the integral in (26) can be written as

$$M(s) = \mathrm{Re}\left\{ \int_0^{+\infty} dx M_c(x) x G(x, s, L) \right\}. \tag{38}$$

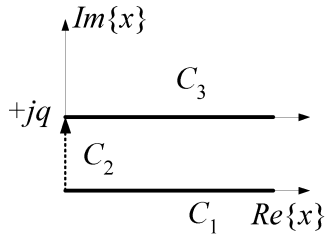

Fig. 2. Deformation of the original contour of integration C_1 (positive real axis) to the contours C_2 and C_3.

To facilitate the numerical calculations, the contour of integration is deformed to a straight line C_3, parallel and above the positive real axis (see Fig. 2). To justify this deformation, we first note that $jtH_0^{(1)}(jt\rho) = 2tK_0(t\rho)/\pi$, where $K_0(x)$ is the modified Bessel function of the second type [9, Ch. 9]. Hence, $jtH_0^{(1)}(jt\rho)$ is real for $t \in \Re$ and the function $G(z, s, \rho)$ in (36) is purely real along the path C_2 of Fig. 2. Since C_2 lies entirely on the imaginary axis, the contribution of the integral along C_2 is purely imaginary. The MGF is the real part of the integral (38) and the contribution of C_2 can be ignored. Hence, the integration can be carried out along $C_3 = \{x + jq, x \geq 0\}$, and $M(s)$ is given by

$$M(s) = \mathrm{Re}\left\{ \int_0^{+\infty} dx M_c(x + jq)(x + jq) G(x + jq, s, L) \right\}. \tag{39}$$

The value of q should be chosen so that the oscillations of the integrand of (39) have the smallest possible amplitude. A likely candidate is the value $q = q_0$ for which $|M_c(jq)G(jq, s, L)|$ becomes minimum. For this value of q, the oscillations of $M_c(z)G(z, s, L)$ along C_3 will start with the minimum amplitude rendering the integrand more suitable for numerical integration. These remarks are better illustrated in Fig. 3. In Fig. 3(a) $\log_{10}|M_c(jq)G(jq, s, L)|$ is plotted for $s = 3$, $c_0 = 0$, $c_1 = \cdots = c_{16} = 0.25$, and it is seen that the value of $q = q_0$ that minimizes $|M_c(jq)G(jq, s, L)|$, is $q_0 \cong 10$. In Fig. 3(b) and (c), the real part of the functions $F_1(x) = xM_c(x)G(x, s, L)$ and $F_2(x) = zM_c(z)G(z, s, L)$ (where $z = j10 + x$) are plotted, respectively. It is clearly seen that the amplitude of the oscillations of $F_1(x)$ is much lower than those of $F_2(x)$. Since, as explained previously, the value of $M(s)$ can be calculated either from the integral of $F_1(x)$ or $F_2(x)$, it is preferable to integrate $F_2(x)$ in order to obtain $M(s)$.

The evaluation of the function $G(x + jq, s, L)$ given by (36) can be easily accomplished using standard numerical integration methods. Then, the function $M(s)$ can be computed numerically using (39) and the computed values of $G(x + jq, s, L)$. For large x, the asymptotic form of $G(z, s, L)$ given in (37) can be used to speed up the computations. This procedure proves to be accurate if the number of interferers M does not exceed 70. As will be shown subsequently if $M > 60$, then the limiting form of $M(s)$ as $M \to \infty$ can be used to approximately estimate the EP.

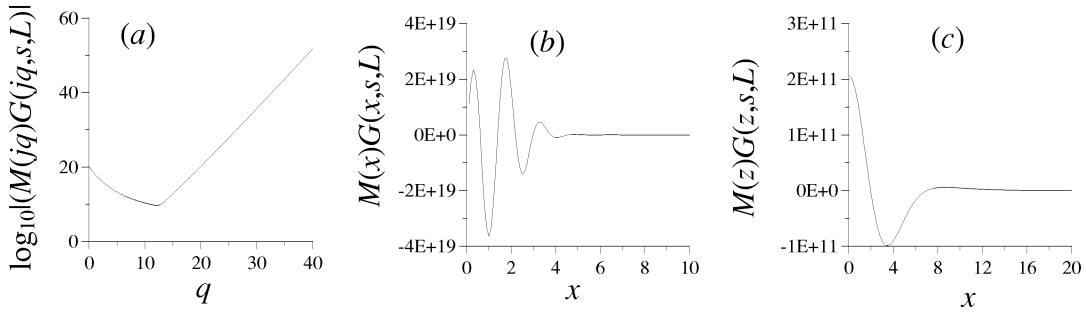

Fig. 3. (a) The function $\log_{10}|M(jq)G(jq,s,L)|$ with respect to q. (b) The function $M(x)G(x,s,L)$ with respect to x. (c) The function $M(x+jq_0)G(x+jq_0,s,L)$ with respect to x. The functions are plotted for $M=16$, $c_0=0$, $c_1=\cdots=c_{16}=0.25$, and $s=3$.

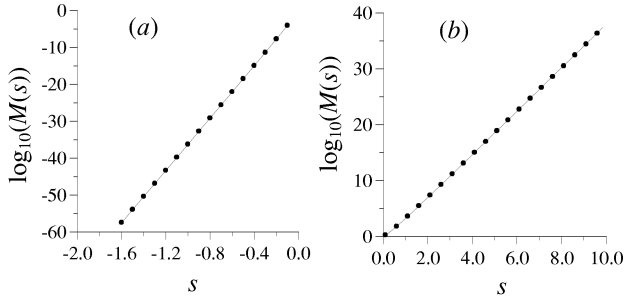

Fig. 4. Logarithmic plot of the numerically computed MGFs (solid lines) and MGFs obtained using (40) (shown with circles) for (a) $M=1$, $s<0$, $c_0=10$, $c_1=1$ and (b) $M=2$, $s>0$, $c_0=0$, $c_1=1$, and $c_2=1$.

V. Accuracy of the Computed MGF

Before the theory developed in the previous sections is applied, it is useful to investigate the validity of the computed MGFs. In the special case where there are only two nonzero amplitudes c_m for $0 \le m \le M$, then $M(s)$ is known in closed form, and a first test is to compare the computed MGFs with their closed forms values. If c_a and c_b denote the two nonzero amplitudes from (9), then D reduces to $D=c_a^2+c_b^2+2c_ac_b\cos(\phi_a-\phi_b)$. Using the fact that the expected value of $\exp(sc_ac_b\cos(\phi_a-\phi_b))$ is $I_0(sc_ac_b)$ [3], it is easily deduced that the MGF is given by

$$M_D(s)=e^{s(c_a^2+c_b^2)}I_0\left(2c_ac_bs\right). \tag{40}$$

In Fig. 4(a), the numerically computed MGF and the MGF of (40) are plotted for $s<0$, for $c_0=c_a=10$ and $c_1=c_b=1$. The same is done in Fig. 4(b) for $s>0$, for $c_1=c_a=2$ and $c_2=c_b=1$. The agreement between (40) and the numerically computed MGFs is excellent in both cases.

In order to test the validity of the computed MGFs in the case where the number of nonzero c_m is larger than two for $s>0$, the MGF obtained with the numerical integration procedure outlined in Section IV-E is plotted Fig. 5, along with the asymptotic MGF (B3) for large s obtained in Appendix B. The MGFs are computed for $c_0=0$ and $c_1=c_2=c_3=1$ in Fig. 5(a), $c_1=\cdots=c_{16}=0.5$ in Fig. 5(b), and $c_1=\cdots=c_{64}=0.1$ in Fig. 5(c). In all three sections of the figure, the numerically computed MGFs eventually converge to their asymptotic values, and this convergence becomes slower as the number of interferers M increases, as explained in Appendix B. The agreement between the asymptotic and the numerical value of the MGF is a strong indication that the numerical integration procedure of Section IV-E produces accurate results.

For $s<0$, the results obtained using the saddle-point approximation and direct numerical integration of (29) along the real axis are compared in Fig. 6, for $s<0$. The numerical integration procedure applied is a slight variation of standard Gaussian quadrature [13]. The integral in $[0,+\infty)$ is approximated by the integral in the interval $[0,x_{\max}]$, where $x_{\max}$ is chosen so that the exponential $\exp(x_{\max}^2/4/s)$ in (29) is below 10^{-40}. This ensures that the value of the integral in $[x_{\max},+\infty)$ is negligible and that the integral in $[0,+\infty)$ can be approximated by the integral in $[0,x_{\max}]$. Next, the zeroes of the integrand are located in the positive real axis inside the interval $[0,x_{\max}]$. The located zeroes $\{x_i\}$ define intervals $X_i=[x_i,\ x_{i+1}]$ in which the integrand is smooth and where Gaussian quadrature can be accurately applied. The value of the integral in $[0,x_{\max}]$ is the sum of the computed values of the integrals in the intervals X_i. It should be noted that this procedure is likely to fail if s is large, in which case the rate of decay of the exponential $\exp(x^2/4/s)$ is slow and the integrand of (29) undergoes many sign changes in $[0,x_{\max}]$. In the computation of the EP by the saddle-point method presented in Section II, the MGF is expected to reach very low values (even below than 10^{-20}). Consequently, a numerical error in the estimation of the integral of the order 10^{-16} (due to roundoff errors, for example) will cause a significant deviation between the computed and the actual value of $M(s)$ if the actual value of $M(s)$ is very small. This is readily seen in Fig. 3, where the results obtained with the saddle-point method and Gaussian quadrature are compared for $c_0=10$ and $c_1=c_2=c_3=1$ in Fig. 6(a), $c_1=\cdots=c_{16}=0.5$ in Fig. 6(b), and $c_1=\cdots=c_{64}=0.1$ in Fig. 6(c). For values of the MGF above 10^{-14}, the results obtained by numerical integration and the saddle-point approximation agree very well, but for lower values, the MGF obtained with numerical integration behaves rather strangely for reasons explained previously. It is therefore preferable to use the saddle-point approximation in order to compute the MGF.

It is also useful to demonstrate that the pdf of D converges to its asymptotic form $f_a(x)$ when $M\to\infty$, which is given by a chi-square distribution [8]

$$f_a(x)=\frac{1}{\sigma^2}\exp\left(-\frac{x+c_0^2}{\sigma^2}\right)I_0\left(\frac{2c_0\sqrt{x}}{\sigma^2}\right) \tag{41}$$

where

$$\sigma^2=\sum_{m=1}^{M}c_m^2. \tag{42}$$

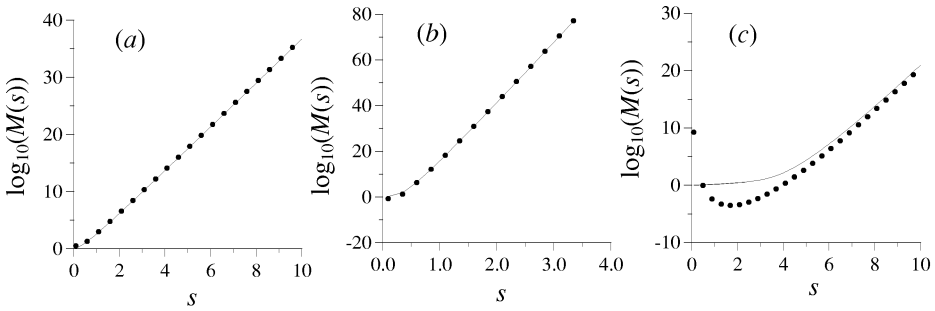

Fig. 5. Logarithmic plot of the asymptotic MGFs (shown with circles) and MGFs calculated by contour deformation and numerical integration (solid lines) for $c_0 = 0$ and : (a) $M = 3$, $c_1 = c_2 = c_3 = 1$; (b) $M = 16$, $c_1 = \cdots = c_{16} = 0.5$; and (c) $M = 64$, $c_1 = \cdots = c_{64} = 0.1$.

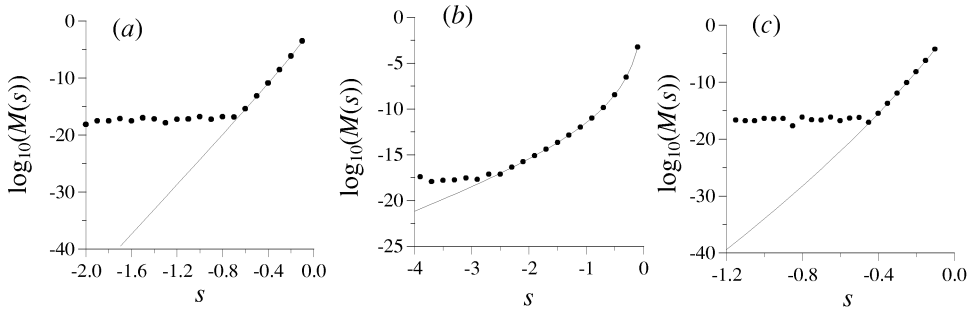

Fig. 6. Logarithmic plot of the MGFs calculated with the saddle-point approximation (solid lines) and numerical integration along the real axis (shown with circles) for $c_0 = 10$ and (a) $M = 3$, $c_1 = c_2 = c_3 = 1$; (b) $M = 16$, $c_1 = \cdots = c_{16} = 0.5$; and (c) $M = 64$, $c_1 = \cdots = c_{64} = 0.1$.

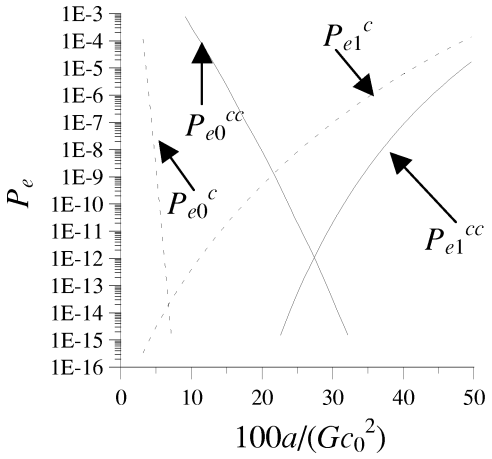

Fig. 7. Convergence of the left tails of the pdf of the decision variable to their asymptotic chi-square form when $M \to \infty$. It is assumed that $c_0 = 10$ and $\sigma^2 = 1$.

In the case of finite M, it is possible to calculate the left tails of the pdf by numerically differentiating the cumulative probability density function (cpdf) of D given by (2). The left tails of the pdf of D for the case $c_0 = 10$, $\sigma^2 = 1$ and $M = 20$, 60 100 180 are plotted in Fig. 7, along with the left tails of the asymptotic pdf obtained using (41). For finite M, it is assumed that the interferers have the same amplitude (i.e., $c_m = c_1$, for $m > 0$). It is deduced that the pdf of D gradually converges to its asymptotic chi-square distribution. In fact, for $M > 180$, the pdf of D is practically indistinguishable from its asymptotic distribution.

VI. Inclusion of ASE and Electrical Noise

In this section, the model will be extended to include the optical amplifier ASE noise and the electrical noise at the receiver. In this paper, it will be assumed that the transfer function of the optical filter following the amplifier is rectangular and that the quantum efficiency of the photodetector is equal to unity. Under these assumptions, the MGF of the decision variable D_a of the amplified system $M_{a|D}(s)$, conditioned on the decision variable of the unamplified system D (measured in photoelectrons) is [4], [8]

$$M_{a|D}(s) = \left(\frac{1}{1-N_0 s}\right)^Q \exp\left(\frac{DGs}{1-N_0 s}\right). \qquad (43)$$

In (43), $N_0 = n_{\rm sp}(G-1)$ is the power spectral density of the ASE noise, while G and $n_{\rm sp}$ are the gain and the spontaneous emission parameter of the optical amplifier, respectively. $Q+1$ is equal to the product BT of the bandwidth B of the optical filter with the bit duration T (Q is assumed to be an integer). Taking the expected value of $M_{a|D}(s)$ with respect to D, one can calculate the MGF $M_a(s)$ of D_a unconditionally of D

$$M_a(s) = E\left\{M_{a|D}(s)\right\} = \left(\frac{1}{1-N_0 s}\right)^Q M\left(\frac{DGs}{1-N_0 s}\right). \qquad (44)$$

It is therefore deduced that the MGF $M_a(s)$ of the optically amplified system can be directly computed from the MGF of the unamplified $M(s)$ system with a simple change of variable $\left(s \to DGs/(1-N_0 s)\right)$ and multiplication with the factor $(1-N_0 s)^{-L}$. Although (44) holds in the case of a rectangular

optical filter, it is easy to obtain an expression similar to (44) for a nonrectangular optical filter, in which case (44) is slightly more complicated [14].

The electrical thermal noise, which is neglected in (44), can easily be incorporated. The thermal noise is assumed a Gaussian additive noise, whose MGF is $\exp(\sigma_{th}^2 s^2/2)$, where σ_{th}^2 is the thermal noise power. Therefore, to include the thermal noise influence, the MGF of the decision variable must therefore be multiplied by $exp(\sigma_{th}^2 s^2/2)$.

VII. Importance of the Crosstalk–Crosstalk Noise

The model presented in the previous sections will now be used to assess the implications of the crosstalk–crosstalk noise in the performance of the system. Assuming a simple nonreturn-to-zero (NRZ) ON–OFF keying, then in the case where the signal bit is $b_s = 1$, the energy of the optical signal (in photons) before the optical amplification will be given by $c_0^2 = P_{\rm in}T/(hf_0)$, where $P_{\rm in}$ is the incident optical power of the signal at the amplifier input, h is Planck's constant, and T the bit duration. In the case where $b_s = 0$, assuming a perfect extinction ratio, $c_0 = 0$. The power of the thermal noise (in photoelectrons$^2/s^2$) is equal to $\sigma_{th}^2 = 2k_B T_K T/(q_e^2 R_L)$ where k_B is Boltzmann's constant, R_L the load resistor of the photodetector, T_K the temperature (in Kelvin), while q_e is the charge of the electron.

In Fig. 8(a), the error probabilities $P_{e,i}^{cc}$ when the crosstalk–crosstalk noise is included and the signal bit is $b_s = i$ are plotted with solid lines for various values of the decision threshold a at the receiver (expressed as a percentage of the number of photoelectrons Gc_0^2 of the signal at the photodiode output in the case $b_s = 1$), assuming that $M = 32$, $P_{\rm in} = -30$ dBm, $G = 30$ dB, $n_{\rm sp} = 1$, $T = 100$ ps (corresponding to a bit rate of 10 Gb/s), $B = 10/T = 100$ GHz, $R_L = 100\ \Omega$, and signal-to-crosstalk ratio $\mathrm{SXR} = 20$ dB, where

$$\mathrm{SXR} = \frac{c_0^2}{\sum_{m\geq 1} c_m^2} \tag{45}$$

is the optical-signal-to-crosstalk ratio, defined as the ratio of the energy of the signal divided by the energy of the crosstalk noise. Also plotted with dashed lines are the error probabilities $P_{e,i}^{c}$ when the crosstalk–crosstalk noise is neglected obtained using the MGF given by (10). The error probabilities predicted by the two models are quite different when $b_s = 0$, since in this case, the signal–crosstalk noise is not present and the crosstalk–crosstalk beating noise becomes a major noise contribution. The difference is also important in the case where the signal bit is $b_s = 1$. It is interesting to note that if $b_s = 1$, the error probability is less if the crosstalk–crosstalk influence is included. This behavior can be justified by considering an unamplified system with $M \to \infty$, in which case the pdf of the decision variable is known in closed form. When the crosstalk–crosstalk influence is included, the pdf $f_a(x)$ of the decision variable D is given by the chi-square distribution (41). When the crosstalk–crosstalk term is ignored, the pdf of D is a Gaussian distribution [8] with a mean value equal to c_0^2 and standard deviation equal to $2c_0^2\sigma^2$. In Fig. 8(b), $f_a(x)$ and $g_a(x)$ are plotted for $c_0 = 10$ and $\sigma^2 = 1$. As seen by the figure, the inclusion of the crosstalk–crosstalk noise changes the statistical behavior of the decision variable, and since the left tails

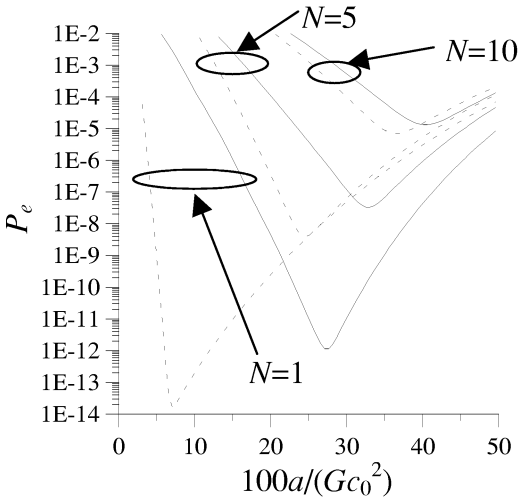

Fig. 8. (a) Error probabilities $P_{e,i}^{cc}$ when the crosstalk–crosstalk noise is included (solid lines) and $P_{e,i}^{c}$ when the crosstalk–crosstalk noise is neglected (dashed lines) with respect to the threshold at the receiver a (expressed as percentage of the input signal energy Gc_0^2 at the receiving photodiode). (b) The asymptotic pdfs $f_a(x)$ and $g_a(x)$ of the unamplified system in the case where $c_0 = 10$ and $\sigma^2 = 1$.

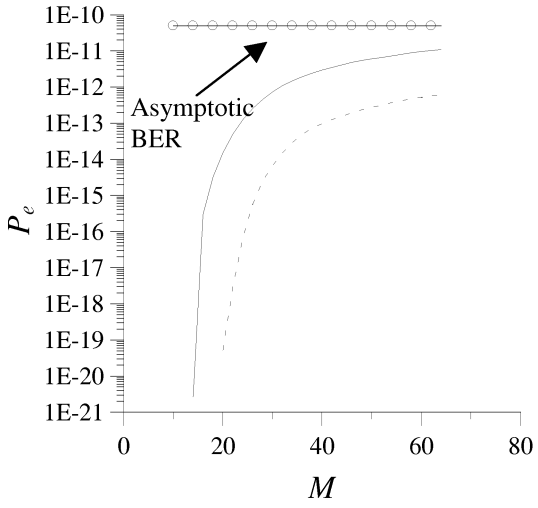

Fig. 9. Variation of the EP with respect to the receiver threshold (expressed as percentage of the input signal energy Gc_0^2 at the receiving photodiode) when the crosstalk–crosstalk noise is included (solid lines) and when it is not (dashed lines), for $M = 32$, $\mathrm{SXR} = 20$ dB, and $P_{\rm in} = -30$ dBm. N is the number of optical amplifiers.

of $f_a(x)$ are below those of $g_a(x)$, P_{e1} will be less when the crosstalk–crosstalk noise is included.

In Fig. 9, the value of the EP of the system obtained as the average of the error probabilities obtained in the cases $b_s = 1$ and $b_s = 0$ are plotted. In the figure, N denotes the number of optical amplifiers that both the signal and the crosstalk components pass, before reaching the photodiode. The power spectral density of the ASE noise is $N_0 = Nn_{\rm sp}(G-1)$. The last amplifier is that of the preamplified receiver,,and in the case $N = 1$, only this amplifier is assumed. The rest of the system parameters are those of Fig. 8(a). For $N = 1$, the optimum threshold predicted by the two models is quite different and the minimum EP also differs in about two orders of magnitude. However, as N begins to increase, the ASE noise accumulates, and the crosstalk–crosstalk noise becomes less important, reducing the

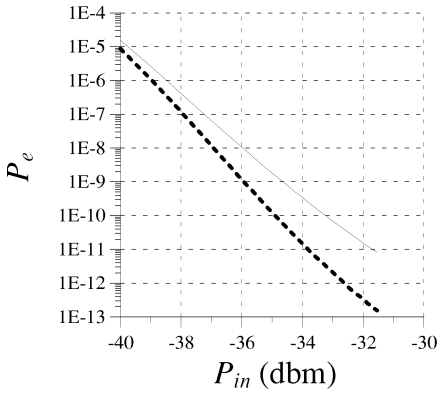

Fig. 10. Variation of the minimum EP with respect to the number of interferers M for constant signal-to-crosstalk ratio $\mathrm{SXR} = 20$ dB when the crosstalk–crosstalk noise is included (solid lines) and when it is not (dashed lines). Also plotted is the asymptotic value of the EP obtained using the model of [8] (circles).

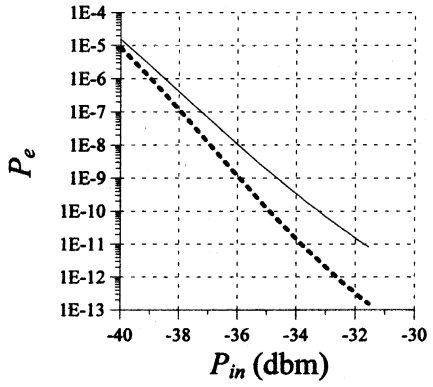

Fig. 11. Variation of the minimum EP with the input power P_{in} when the crosstalk–crosstalk noise is included (solid lines) and when it is not (dashed lines), for $M = 32$ interfering channels and $\mathrm{SXR} = 20$ dB.

difference between the two models. The difference in the EP is about one order of magnitude for $N = 5$. The value of the optimum threshold (i.e., the threshold for which the EP is minimum) is also quite different for the two models. For $N = 10$, the ASE noise dominates, and the value of the minimum EP is approximately the same for the two models.

The variation of the minimum EP, when the crosstalk–crosstalk contribution is included (solid line) and when it is ignored (dashed line), with the number of interferers M for SXR constant and equal to 20 dB is also plotted in Fig. 10. As seen by the figure, the difference between the predicted values of the EP is about two orders of magnitude for $M > 20$. Also plotted in the figure is the asymptotic value of the EP when the crosstalk–crosstalk noise is included, which is calculated with the asymptotic MGF ($M \to \infty$) [8] and was found to be 5.0×10^{-11}. As seen in the figure, the EP gradually converges to its asymptotic value. For $M = 64$, the EP using the model of the present paper was estimated to be about 1.3×10^{-11}. This implies that for $M > 64$, the EP will be of the same order of magnitude compared to the EP obtained by the asymptotic model ($M \to \infty$).

The difference between the two models is further illustrated in Fig. 11, where the value of the EP is plotted as a function of the input power for $M = 32$, assuming that the optical SXR remains constant and equal to $\mathrm{SXR} = 100$. This assumption is made since, in most networks (such as an AWG interconnection [3]), the power of the crosstalk noise is proportional to the power of the signal, and therefore increasing the input power does not alter the value of the SXR. By comparing the values of P_{in} required to achieve an EP equal to 10^{-9}, it is deduced that the inclusion of the crosstalk–crosstalk noise causes a power penalty of about 1.3 dB. Hence, the crosstalk–crosstalk noise can become an important issue in system design.

VIII. Conclusion

In this paper, an accurate method for the estimation of the EP in the presence of in-band crosstalk in a WDM receiver was presented. This model is based on the formulation of the MGF of the decision variable in terms of a double integral. This formulation allows the inclusion of the crosstalk–crosstalk noise, which was neglected in previous models. The model was extended to include the ASE noise of the optical amplifiers and the thermal noise at the receiver. Using this model, the importance of the crosstalk–crosstalk noise in the performance of the system was investigated, and it was shown that the crosstalk–crosstalk noise can have an important bearing in the performance of the system, since it influences the value of the optimum threshold, the minimum EP and can also introduce some power penalties.

Appendix A
Derivation of the Asymptotic Form of $G(z, s, l)$

To obtain an asymptotic form for $G(z, s, L)$, we use the integration by parts technique frequently employed for the asymptotic expansion of integrals [12]. Since $(\rho H_1(z\rho))' = \rho H_0^{(1)}(z\rho)$, integral (36) can be written as

$$G(z,s,L) = \left[\frac{\rho}{z} e^{\rho L^2} H_1^{(1)}(z\rho)\right]_0^L - \frac{2s}{z}\int_0^L d\rho \rho^2 H_1^{(1)}(z\rho) e^{s\rho^2}. \tag{A1}$$

Applying de L'Hopital's rule, one can show that $H_1^1(z\rho)/\rho \to -j/z$. Using the integration by parts technique once again, it is also possible to show that the remainder integral in (A1) is $O(x^{-5/2})$. Hence, for large z, $G(z, s, L)$ behaves as

$$G(z,s,L) \cong \frac{L}{z} H_1^{(1)}(zL) e^{sL^2} + j\frac{2}{z^2}. \tag{A2}$$

Appendix B
Derivation of the Asymptotic Form of $M(s)$ For Large S

Using (11), one can derive an asymptotic expression for the MGF of the decision variable for large values of s using the theory of [12, Ch. 4]. Let the function Q be defined as

$$Q(\phi_1, \ldots, \phi_M) = \sum_{mn=0}^{M} c_m c_n \cos(\psi_m - \psi_n). \tag{B1}$$

Then (11) can be written as

$$M(s) = \frac{1}{(2\pi)^M} \int_{-\pi}^{\pi} d\phi_1 \cdots \int_{-\pi}^{\pi} d\phi_M \exp\left(sQ\left(\psi_1, \ldots, \psi_M\right)\right). \tag{B2}$$

To find the asymptotic expansions (B2), one must locate the critical points of Q where $\nabla Q = 0$. The most important critical point is $\psi_1 = \cdots = \psi_M = 0$, where Q obtains its highest value $Q(0, \ldots, 0) = L^2$. Neglecting the contribution of the other critical points of Q (such as $\psi_j = \pi$ and $\psi_p = 0$ for $p \neq j$, etc.), then for large s, the first-order term in the asymptotic expansion of (B2) is given by

$$M(s) \cong \frac{1}{(2\pi)^M} \exp\left(sL^2\right) \frac{1}{|\det(J)|^{1/2}} \tag{B3}$$

where the elements of the matrix $J = [J_{kl}]$ are the partial derivatives $J_{kl} = \partial^2 Q / \partial\psi_k \partial\psi_l$ calculated at $\psi_1 = \cdots = \psi_M = 0$. It should be noted that (B3) is the contribution of the most important critical point. As M increases, however, so does the total number of the critical points, and as a result, the convergence of $M(s)$ to its asymptotic form (B3) may be slower, as shown in Fig. 5.

REFERENCES

[1] C. A. Brackett, "Dense wavelength division multiplexing networks: Principles and applications," *IEEE J. Select. Areas Commun.*, vol. 8, pp. 948–964, Aug. 1990.

[2] E. Iannone, R. Sabella, M. Avattaneo, and G. d. Paolis, "Modeling of in-band crosstalk in WDM optical networks," *J. Lightwave Technol.*, vol. 17, pp. 1135–1141, July 1999.

[3] T. Kamalakis and T. Sphicopoulos, "Application of the saddle point method for the evaluation of crosstalk implications in an arrayed waveguide grating interconnection," *J. Lightwave Technol.*, vol. 20, pp. 1357–1366, Aug. 2002.

[4] G. Einarsson, *Principles of Lightwave Communications*. New York: Wiley, 1996.

[5] K. P. Ho, "Analysis of homodyne crosstalk in optical networks using Gram–Charlier series," *J. Lightwave Technol.*, vol. 17, pp. 149–154, Feb. 1999.

[6] I. T. Monroy and E. Tangliongga, "Perfomance evaluation of optical crossconnects by saddlepoint approximation," *J. Lightwave Technol.*, vol. 16, pp. 317–323, Mar. 1998.

[7] X. Jiang and I. Roudas, "Asymmetric probability density function of a signal with interferometric crosstalk," *IEEE Photon. Technol. Lett.*, vol. 13, pp. 160–162, Feb. 2001.

[8] T. Kamalakis and T. Sphicopoulos, "Asymptotic behavior of in-band crosstlalk noise in WDM networks," *IEEE Photon. Technol. Lett.*, vol. 15, pp. 476–478, Mar. 2003.

[9] A. Abramowitz and I. Stegun, *Handbook of Mathematical Functions*, 9th ed. New York: Dover.

[10] I. S. Gradshteyn and I. M. Ryzhik, *Table of Integrals Series and Products*, 6th ed. New York: Academic.

[11] L. B. Felsen and N. Marcuvitz, *Radiation and Scattering of Waves*. Englewood Cliffs, NJ: Prentice-Hall, 1973.

[12] N. G. de Brujin, *Asymptotic Methods in Analysis*. New York: Dover, 1981.

[13] F. B. Hildebrand, *Introduction to Numerical Analysis*. New York: Dover.

[14] E. Forestieri, "Evaluating the error probability in lightwave systems with chromatic dispersion, arbitrary pulse shape and pre- and postdetection filtering," *J. Lightwave Technol.*, vol. 18, pp. 1493–1503, Nov. 2000.

Thomas Kamalakis, photograph and biography not available at the time of publication.

Thomas Sphicopoulos (M'87), photograph and biography not available at the time of publication.

Manolis Sagriotis, photograph and biography not available at the time of publication.